

Exploring Ultralight Dark Matter Self-Coupling via the Gravitational Wave Background

Pratick Sarkar^{✉*}

*School of Physical Sciences, Indian Association for the Cultivation of Science,
2A & 2B Raja S.C. Mullick Road, Kolkata-700032, India*

Supermassive black hole binary mergers serve as prominent sources of the stochastic gravitational wave background (SGWB), detectable by pulsar timing arrays (PTAs). If dark matter-induced friction is present in the vicinity of these mergers, it can lead to suppression in the nanohertz frequency range of the SGWB spectrum. In particular, ultralight dark matter (ULDM) forming compact solitonic cores around supermassive black holes can imprint signatures in PTA observations. Our analysis places limits on the mass and self-interaction strength of ULDM, demonstrating that soliton-induced dynamical friction can significantly alter the SGWB spectrum. PTAs have the potential to exclude certain ULDM mass ranges while probing the effects of self-interactions, offering a novel avenue to investigate the fundamental properties of ULDM.

I. INTRODUCTION

Compelling experimental evidence, such as galaxy rotation curves, gravitational lensing, and the cosmic microwave background, strongly supports the existence of dark matter (DM)[1–5]. There are numerous reasons to believe that the universe is structured with a non-relativistic, non-baryonic component that does not emit light[6]. Understanding the nature of this component is one of the major challenges in cosmology and astrophysics[7, 8]. Extensive efforts have been made, including direct and indirect searches[9–12] as well as collider studies[13], to investigate DM. One prevailing theory posits that DM consists of collision-less, non-relativistic bosons or fermions, collectively referred to as Cold Dark Matter (CDM)[6]. This model works well on large scales (on the order of hundreds of Mpc). However, on smaller scales, some observations deviate from this picture. For example, the core-cusp problem — where DM-only simulations predict dense, cuspy halos at galactic centers in contrast with the observed cored density profiles[14–17]. The absence of definitive results from DM detection experiments, combined with these small-scale discrepancies, has motivated the exploration of alternative models beyond the conventional CDM paradigm.

An intriguing alternative considers ultralight dark matter (ULDM), consisting of bosons with masses on the order of $\sim 10^{-22}$ eV[18, 19], often called fuzzy dark matter (FDM). Such particles could occupy a large volume due to their long de Broglie wavelength, on the order of kilo parsecs, exhibiting wavelike behavior at galactic scales[20]. This wavelike nature of ULDM particles introduces quantum pressure effects that can counteract gravitational collapse, thereby preventing the formation of cuspy density profiles[18, 21–23]. At the centers of dark matter halos, ULDM particles can give rise to stable and dense configurations—referred to as soliton

cores[24, 25]—which are, however, less dense than the cuspy profiles typically expected in standard CDM scenarios.

The centers of galaxies harbor massive black holes which again influence the soliton core formation. The ULDM that forms this soliton core is expressed by a scalar field. The problem of a scalar field having self-interaction, minimally coupled in the gravitational influence of a black hole, is described by the coupled Gross-Pitaevskii-Poisson equations and has been studied extensively in the literature[26–29]. These coupled equations are based on a weak-field, slowly varying, non-relativistic canonical scalar field model for ULDM particles.

Recent studies have focused on ULDM with self-interactions, as explored in works such as [30–32]. In such models, determining observational constraints on the mass(m) and self coupling(λ) of ULDM that forms the soliton core is critically important.

The detection of the stochastic gravitational wave background (SGWB) through pulsar timing array (PTA) observations can provide evidence of supermassive black hole (SMBH) binary mergers. Currently, several major PTA collaborations are actively searching for SGWB signals. These include the European Pulsar Timing Array (EPTA)[33, 34], Parkes Pulsar Timing Array (PPTA)[35–37], North American Nanohertz Observatory for Gravitational Waves (NANOGrav)[38, 39], the Indian Pulsar Timing Array (InPTA)[33], the Chinese Pulsar Timing Array (CPTA)[40], and the International Pulsar Timing Array (IPTA)[41], which combines data from multiple PTA experiments. PTAs rely on precise timing measurements of highly stable millisecond pulsars to detect variations in the propagation of light caused by gravitational waves (GWs).

The SGWB observed by PTAs aligns well with expectations from inspiraling SMBH binaries[42, 43]. These SMBHs, with masses ranging from $10^5 M_\odot$ to $10^{10} M_\odot$, are typically found at the centers of galaxies. During hierarchical structure formation, galaxy mergers may lead to the formation of SMBH binaries. In the final stages of their evolution, these binaries emit gravitational waves

* spsps2523@iacs.res.in

in the nanohertz frequency band, which fall within the sensitivity range of current PTA observations. If binary evolution is driven solely by the loss of orbital energy through GW emission, the SGWB can be described by a characteristic strain h_c with a power-law dependence on frequency, $h_c(f) \propto f^{-2/3}$ [44]. However, realistic modeling of the astrophysical environments surrounding the binaries suggests modifications to this power-law[45, 46]. Beyond purely astrophysical effects, deviations in the power-law index of the SGWB, driven by new physics scenarios near SMBH binaries, can be explored. In particular, the presence of a dense ULDM environment, such as soliton cores, induces friction on black hole binary, influencing the generation of the SGWB. At the later stages of a merger event, when the separation between the SMBHs becomes smaller than the soliton radius, both black holes experience a wind of ULDM particles. This phenomenon, known as dynamical friction[47], introduces a novel energy loss mechanism that can compete with gravitational wave emission in the nanohertz frequency range. Consequently, the presence of soliton cores alters the SGWB spectrum. Current PTA data can provide constraints on the modified power-law index of the SGWB, placing limits on the ULDM mass(m), self coupling(λ) and soliton mass.

The structure of the paper is as follows: Section II introduces solitons, formed from ULDM particles around SMBHs. This section discusses the fundamental approach to solving the Gross-Pitaevskii-Poisson equation and deriving solitonic DM profiles. The impact of solitonic DM on the gravitational wave spectrum is explored in Section III. The results are presented in Section IV, and the conclusions are drawn in Section V.

Throughout the paper, we frequently use natural units ($c = \hbar = 1$) but retain c and \hbar explicitly in some of the expressions. The reduced Planck mass is denoted by M_{pl} i.e. $M_{pl} = \sqrt{c\hbar/8\pi G_N} \approx 2.4 \times 10^{18} \text{ GeV}$. The symbol M_\odot denotes the solar mass, which is $M_\odot \approx 2 \times 10^{30} \text{ kg}$.

II. ULDM SOLITON AROUND CENTRAL SMBH

The literature study of ULDM suggests the existence of a dense, macroscopic core at the center of galaxies, commonly known as a soliton[20, 48–51]. This form of dark matter, characterized by an extremely high occupation number, behaves as a classical scalar field and is governed by the wave equation[52, 53]. The classical field theory action for this scalar field ϕ , is given by

$$S = \int d^4x \sqrt{-g} \left(\frac{M_{pl}^2}{2} R - \frac{1}{2} g^{\mu\nu} \partial_\mu \phi \partial_\nu \phi - U(\phi) \right) \quad (1)$$

where the potential has the form

$$U(\phi) = \frac{m^2 \phi^2}{2} + \frac{\lambda \phi^4}{4!} \quad (2)$$

The coefficient λ here denotes the self-coupling parameter of the ULDM particles.

By varying the action with respect to ϕ , we obtain the equation of motion:

$$\partial_\alpha (\sqrt{-g} g^{\alpha\beta} \partial_\beta \phi) = \sqrt{-g} U'(\phi) \quad (3)$$

where $U'(\phi)$ denotes the derivative of the potential with respect to ϕ . R is the Ricci scalar, and g denotes $\det(g_{\mu\nu})$.

Strong evidence suggests that all large galaxies, and even dwarf galaxies, harbor a central SMBH[54–56]. ULDM particles can host this SMBH, feeding from it and evolving into a macroscopic soliton[57–61]. The system of an SMBH embedded within a scalar field dark matter halo is often described using a spherically symmetric metric[62–64], with the Schwarzschild metric being a simplest example.

Alternatively, the cosmological ULDM scalar field can be analyzed by adopting the perturbed FRW metric, as discussed in [24, 48]. In galactic dynamics, the effects of cosmic expansion are negligible. Therefore, we can set the scale factor to unity and the Hubble parameter to zero, leading to the following metric:

$$ds^2 = -(1 + 2\Phi)(dx^0)^2 + (1 - 2\Phi)\delta_{ij} dx^i dx^j \quad (4)$$

within the weak gravity limit, $\Phi \ll 1$, where the Newtonian potential Φ dominates the gravitational influence.

Under this metric, the equation of motion simplifies to:

$$\partial_0^2 \phi - \nabla^2 \phi + U'(\phi) = 2\Phi(2\partial_0^2 \phi + U'(\phi)) \quad (5)$$

Considering ULDM as a massive scalar field ϕ , which satisfies the above Klein-Gordon equation and is minimally coupled to gravity, in the non-relativistic limit can be expressed as [20, 48],

$$\phi(t, \vec{x}) = \frac{1}{\sqrt{2m}} (e^{-imt} \Psi(t, \vec{x}) + c.c.) \quad (6)$$

where m represents the mass of the scalar field, and $\Psi(t, \vec{x})$ encapsulates its dynamical behavior. Here, the complex field Ψ varies slowly in both space and time, satisfying the conditions $|\nabla \Psi| \ll m|\Psi|$, $|\dot{\Psi}| \ll m|\Psi|$ and $|\ddot{\Psi}| \ll m|\dot{\Psi}|$.

In the regime of weak gravity and slowly varying fields, Ψ satisfies the Gross-Pitaevskii-Poisson (GPP) equation[20, 25–28, 50, 51, 65]:

$$i \frac{\partial \Psi}{\partial t} = -\frac{\nabla^2 \Psi}{2m} + m\Phi \Psi + \frac{\lambda}{8m^3} |\Psi|^2 \Psi \quad (7)$$

$$\nabla^2 \Phi = 4\pi G_N |\Psi|^2 \quad (8)$$

We seek spherically symmetric steady-state solutions, assuming an ansatz for¹ $\Psi(t, r) = \chi(r)e^{-i\gamma t}$, where the

¹ $\Psi(t, \vec{x}) = \chi(\vec{x})e^{-i\gamma t}$ and for spherical symmetry $\chi(\vec{x}) = \chi(r)$

ULDM density is given by $\rho(r) = \chi^2(r)$. The solution $\chi(r)$ is real, spherically symmetric, spatially localized, and without nodes. These solutions are known as solitons. The influence of a central black hole is incorporated via the term $m\Phi\Psi = m(V + \Phi_{BH})\Psi$, where V includes the self-potential and the black hole potential is given by, $\Phi_{BH} = -\frac{G_N M_{BH}}{r}$. Here, M_{BH} is the black hole mass, and G_N is Newton's constant. In the absence of self-interactions, the system is usually referred to as Schrödinger-Poisson system.

To solve the coupled equations numerically, we introduce dimensionless variables[50]: distance $\hat{r} = \frac{r}{\hbar/mc}$, wave function $\hat{\chi} = \frac{\sqrt{4\pi G_N \hbar}}{mc^2} \chi$, potential $\hat{V} = V/c^2$, eigen energy $\hat{\gamma} = \gamma/mc^2$. We also define dimensionless parameters for the black hole,

$$\hat{\alpha} = \frac{G_N M_{BH} m}{c\hbar} \quad (9)$$

and for the self interaction,

$$\hat{\lambda} = \frac{\lambda}{8} \left(\frac{m}{M_{pl}} \right)^{-2} = \left(\frac{\lambda}{1.35 \times 10^{-96}} \right) \left(\frac{m}{10^{-21} \text{eV}} \right)^{-2} \quad (10)$$

Using the dimensionless variables, the GPP equation takes the form

$$\begin{aligned} \hat{\gamma}\hat{\chi} &= \left(-\frac{1}{2}\hat{\nabla}^2 + \hat{V} - \frac{\hat{\alpha}}{\hat{r}} + 2\hat{\lambda}\hat{\chi}^2 \right) \hat{\chi}, \\ \hat{\nabla}^2\hat{V} &= \hat{\chi}^2. \end{aligned} \quad (11)$$

Here, the parameters $\hat{\alpha}$ and $\hat{\lambda}$ are free and chosen to solve the system. The parameter $\hat{\gamma}$ is determined using a shooting method by applying boundary conditions to find solutions without nodes[66]. For numerical work, we impose $\hat{\chi}(\hat{r} = 0) \sim 1$ along with the boundary conditions: $\hat{\chi}(\hat{r} = \infty) = 0$, $\hat{\chi}'(\hat{r} = 0) = 0$, $\hat{V}(\hat{r} = 0) = 0$, $\hat{V}'(\hat{r} = 0) = 0$. Although $\hat{\chi}(\hat{r} = 0) = 0$ may also yield solutions, these are not realistic for modeling physical soliton profiles, since the other dimensionless parameters are $\mathcal{O}(1)$. Details of the numerical procedure are provided in the Appendix A.

For each unique solution, the total mass of the soliton is given by

$$\begin{aligned} M &= \frac{\hbar c}{G_N m} \int_0^\infty \hat{\chi}^2 \hat{r}^2 d\hat{r} \\ &= 1.33 \times 10^{11} M_\odot \left(\frac{10^{-21} \text{eV}}{m} \right) \int_0^\infty \hat{\chi}^2 \hat{r}^2 d\hat{r}. \end{aligned} \quad (12)$$

In dimensionless units, the soliton mass is expressed as

$$\hat{M} \equiv \frac{G_N M m}{\hbar c} = \int_0^\infty \hat{\chi}^2 \hat{r}^2 d\hat{r}. \quad (13)$$

The central ULDM density is derived from $\chi = \frac{mc^2}{\sqrt{4\pi G_N \hbar}} \hat{\chi}$ which is given by

$$\rho = 2(M_{pl} m)^2 \hat{\chi}^2 \sim 10^{16} \left(\frac{m}{10^{-21} \text{eV}} \right)^2 \hat{\chi}^2 M_\odot / \text{pc}^3, \quad (14)$$

Here this value is estimated without taking self-interactions. This density corresponds to a very large mass within a volume of $(\text{pc})^3$. Consequently, solutions assuming $\hat{\chi}(\hat{r} = 0) \sim 1$ yield excessively high densities.

In the absence of a central SMBH, setting $\hat{\alpha} = 0$ in the GPP equation, the Poisson equation implies $\hat{V} \sim \hat{L}^2 \hat{\chi}^2$ for a system of size \hat{L} (in units of \hbar/mc). This leads to $\hat{L} \sim \hat{\chi}^{-1/2}$. If $\hat{\chi} \leq 1$, then \hat{L} remains $\mathcal{O}(1)$. In dimensionful units without the central BH the size of the soliton will be of the order of ULDM Compton wavelength, \hbar/mc (i.e. $\frac{\hbar}{mc} \times \hat{L}$).

When a central BH is present ($\hat{\alpha} > 0$), for $\hat{\alpha} \ll 1$, the $\hat{V}\hat{\chi}$ term dominates over $\frac{\hat{\alpha}}{\hat{r}}\hat{\chi}$ in the GPP equation, keeping the soliton size $\mathcal{O}(1)$. When $\frac{\hat{\alpha}}{\hat{r}}\hat{\chi}$ dominates, the size becomes $\hat{L} \sim 1/\hat{\alpha}$, which requires $\hat{\alpha}$ to be at least $\mathcal{O}(1)$. Thus, the dimensionless size \hat{L} remains $\mathcal{O}(1)$ in either case.

The soliton mass, determined from Eq. 13, is $\mathcal{O}(1)$ in dimensionless units, corresponding to a physical mass of $10^{11} M_\odot$, which exceeds the typical mass of a soliton in galaxies within the mass range of $M_{halo} \sim (10^{12} - 10^{13}) M_\odot$. The gravitational radius of the soliton is

$$R_G = \frac{G_N M}{c^2} = \hat{M} \frac{\hbar}{mc} \sim \frac{\hbar}{mc}, \quad (15)$$

comparable to the soliton size. Real solitons are expected to be larger, less dense, and much lighter. Mapping these estimated soliton densities and sizes to physical values requires scaling of the solutions and parameters in the GPP equation, which is discussed in the next section.

A. Scaling relation

The GPP system of equations has the scaling symmetry[20, 50, 65]

$$\begin{aligned} \hat{\chi} &\rightarrow \frac{1}{s^2} \hat{\chi}, & \hat{V} &\rightarrow \frac{1}{s^2} \hat{V}, & \hat{\alpha} &\rightarrow \frac{1}{s} \hat{\alpha}, & \hat{\gamma} &\rightarrow \frac{1}{s^2} \hat{\gamma}, \\ \hat{r} &\rightarrow s \hat{r}, & \hat{\lambda} &\rightarrow s^2 \hat{\lambda}, & \hat{M} &\rightarrow \frac{1}{s} \hat{M} \end{aligned}$$

s being a scaling parameter, which can be used to transform the dimensionless numerical solutions and parameters to their dimensionful physical values. Each of the term in GPP equation as well as the density scales as $1/s^4$. The ratio of the soliton mass and the black hole mass, M/M_{BH} is invariant under the scaling and is the primary parameter which stabilizes the shape of the soliton. In the limit $M/M_{BH} \lesssim 0.3$, we will get exponential solution just like a hydrogen atom when soliton profile is dominated by the BH gravity[50].

Now we have to model the density profile of the soliton for a given halo mass as a function of ULDM mass using the numerical solutions as discussed in Appendix A.

Over cosmic timescales, the stability of the solitonic core at the center of a galaxy depends on whether it can resist being accreted by the central SMBH. For ULDM

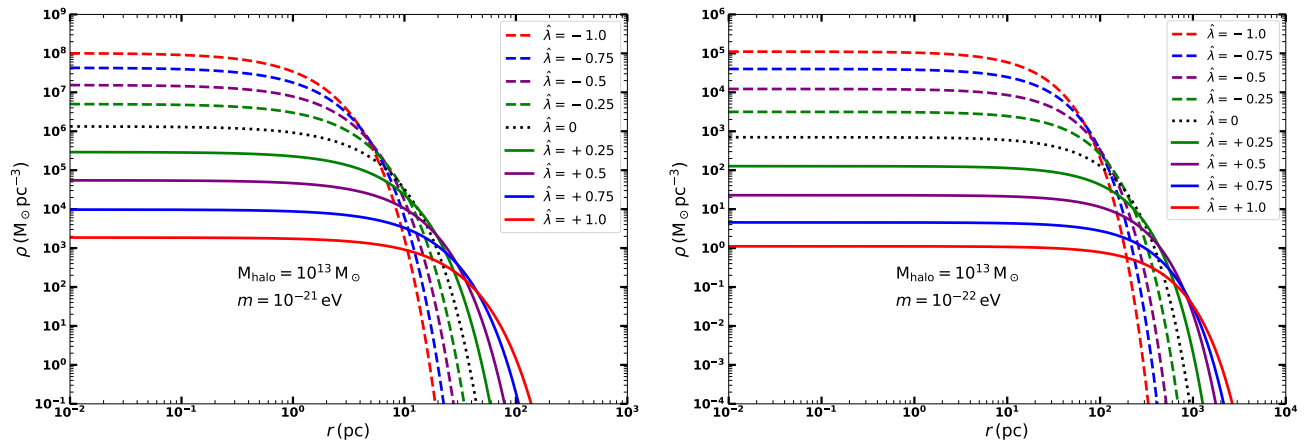


FIG. 1: Numerical solutions to the GPP equation are presented for a halo mass of $10^{13}M_{\odot}$ and ULDM masses of 10^{-21}eV (Left) and 10^{-22}eV (Right). The DM density profiles, shown in different colors, illustrate the effect of varying the dimensionless self-coupling parameter $\hat{\lambda}$, each with distinct characteristic signatures. The GPP equation was solved in dimensionful units, incorporating the gravitational influence of the SMBH through the appropriate values of the $\hat{\alpha}$ parameter corresponding to the given halo mass.

particles, the timescale for this accretion is given by [67, 68],

$$t_{accr} = 5.6 \times 10^{12} \text{yr} \left(\frac{M_{\text{BH}}}{10^8 M_{\odot}} \right)^{-5} \left(\frac{m}{10^{-21}} \right)^{-6} \quad (16)$$

To ensure the solitonic core still exists today, this accretion timescale² must be longer than the current age of the Universe (~ 13.8 Gyr). Since $t_{accr} \propto m^{-6}$, increasing the mass of the ULDM significantly shortens the accretion time. Therefore, requiring that the soliton has not yet been absorbed by the SMBH leads to an upper bound on the ULDM particle mass.

Once the SMBH completes its growth, it may dominate the central mass of the halo, exerting a perturbing force on the system's center. For a DM-only simulations, the mass of the soliton M_{sol} is related to the galactic halo mass via the relation[69]

$$M_{sol} = 2.67 \times 10^8 \left(\frac{M_{halo}}{10^{13} M_{\odot}} \right)^{1/3} \left(\frac{m}{10^{-21} \text{eV}} \right)^{-1} M_{\odot} \quad (17)$$

Nevertheless, this relation is obtained in the absence of SMBHs, the simulation performed by fixing the ULDM mass $m = 10^{-22}\text{eV}$, and halo mass $M_{halo} = (10^9 - 5 \times 10^{11})M_{\odot}$.

As discussed in Appendix A, we took the parameter $\hat{\alpha}$ that produces a solution consistent with the predicted soliton mass for the given halo mass. Next, we convert the dimensionless density profile into physical units and

apply the scaling symmetry to adjust the soliton solution, so that its total mass aligns with the soliton-halo mass relation. This is done by comparing the mass of the scaled numerical solution to the soliton-halo mass relation in Eq. 17 for the given halo mass. The corresponding scaling factor is given by

$$s = \frac{c\hbar}{G_N m M_{sol}} \hat{M} = \frac{1.33 \times 10^{11}}{2.67 \times 10^8} \left(\frac{M_{halo}}{10^{13} M_{\odot}} \right)^{-1/3} \hat{M} \quad (18)$$

Then using this s , we can scale the numerical solutions and other relevant quantities discussed above. For every initial value of $\hat{\lambda}$, we will get the s parameter for chosen $\hat{\alpha}$. The variation of scaling, s with respect to $\hat{\lambda}$ is shown in Appendix B. For attractive self interactions, s parameter getting larger in comparison to repulsive self interaction. This is obvious as the attractive self interaction makes the soliton core more dense and less in size as shown in Fig. 1

Our study is confined to solitons composed of ULDM particles with masses in the range $\sim (10^{-22} \text{ eV} - 10^{-21} \text{ eV})$. We further restrict our analysis to galaxies with halo masses of $M_{halo} \sim 10^{13} M_{\odot}$.

B. Density Profiles

In addition to the soliton-halo mass relation, the SMBH mass is also correlated with the halo mass according to [70], dictated as follows:

$$\log_{10}(M_{\text{BH}}/M_{\odot}) = 8.18 + 1.55[\log_{10}(M_{halo}/M_{\odot}) - 13.0] \quad (19)$$

allowing us to predict the mass of the SMBH and the soliton core for a given halo mass. Assuming the soliton-

² Further refinement in the time-dependent theoretical modeling of this scenario remains an open avenue for improvement.

halo mass relation holds true in the presence of an SMBH—treated as a perturber to the soliton-halo system, the gravitational potential of the SMBH modifies the soliton density profile.

We compute the density profiles in the presence of the SMBH, incorporating its influence through the parameter α . The coupled GPP equation, with fixed halo mass, M_{halo} and the parameter α , are solved numerically using appropriate boundary conditions. These calculations yield density profiles for various values of the λ parameter while keeping α constant. From these solutions, the density is obtained by squaring the soliton solution χ . The ULDM density in physical units is then given by

$$\rho = 4.1 \times 10^{16} \left(\frac{m}{10^{-21}} \right)^2 \hat{\chi}^2 M_{\odot} / pc^3 \quad (20)$$

Finally, we apply the scaling symmetry relations detailed in the Appendix B to rescale the soliton density so that its total mass matches the value predicted by the soliton-halo mass relation.

Fig. 1 displays the density profiles for different values of $\hat{\lambda}$ while keeping the halo mass fixed at $10^{13} M_{\odot}$. The left panel corresponds to a ULDM mass of 10^{-21}eV while the right panel represents profiles for a ULDM mass of 10^{-22}eV . As shown in the figure, an attractive self-coupling ($\hat{\lambda} < 0$) results in more compact solitons—denser and smaller in size (dashed curves). In contrast, a repulsive self-coupling ($\hat{\lambda} > 0$) leads to solitons that are less dense and larger in size (solid curves). The black dotted lines represent solitons with no self-coupling between ULDM particles.

III. DM INFLUENCE ON GRAVITATIONAL WAVE BACKGROUND

In this section, we examine the gravitational wave frequency spectrum emitted during the merger of SMBH binaries, considering the influence of ULDM [71, 72]. We analyze a system with two black holes of masses M_1 and M_2 , orbiting in a circular path with radius r , an angular velocity ω , and velocity v . The dominant mechanism for energy loss depends on the separation: at smaller r , gravitational wave emission is the primary source, while at larger r , interactions with surrounding matter, including dark matter friction, become significant. The GW spectrum exhibits a transition in its slope when these two energy loss mechanisms contribute comparably.

At the nanohertz frequency range observed by PTAs, SMBH binaries are widely separated compared to their Schwarzschild radius, which is given by $R_{\text{Sch}} = 2G_N M_1$, M_1 being one of the SMBH mass. The binary motion remains in the Newtonian regime with $v \ll 1$. Assuming circular orbits, the radial acceleration satisfies:

$$\frac{v^2}{r} = \omega^2 r = \frac{G_N (M_1 + M_2)}{r^2}. \quad (21)$$

From this, the orbital velocity follows as $v = \omega r \sim \sqrt{R_{\text{Sch}}/r} \ll 1$ for approximately equal-mass binaries.

The frequency of the emitted GWs in the source frame is

$$f_s = \frac{\omega}{\pi}, \quad (22)$$

where the absence of a factor of 2 reflects the spin-2 nature of gravitational waves. For a source at redshift z , the observed frequency is related by

$$f = \frac{f_s}{1+z}. \quad (23)$$

Two primary mechanisms contribute to the orbital energy loss:

- **Gravitational Wave Emission:** The power radiated via GW emission is given by [73]

$$\mathcal{W}_{GW} = \frac{32}{5} G_N \mu^2 \omega^6 r^4, \quad (24)$$

where $\mu = \frac{M_1 M_2}{M_1 + M_2}$ represents the reduced mass. This follows from the quadrupole radiation of gravity waves. Systems with larger black holes (considering $M_1 \sim M_2$) dominate this radiation.

- **Dynamical Friction from ULDM:** Another process of energy loss is the dynamical friction which occurs when a mass (SMBH in our case) moves in a background of ULDM particles. According to the studies [47, 74] the force exerted by dynamical friction on a black hole moving through a ULDM background is given by

$$F_{DF} = \frac{4\pi G_N^2 \mu^2 \rho}{v_{rel}^2} C_{cl}(\Lambda). \quad (25)$$

Here, v_{rel} denotes the relative velocity between the black hole and ULDM particles, ρ represents the local ULDM density, and $C_{cl}(\Lambda) = \ell p$ accounts for gravitational feedback effects [71]. Here $\ell \approx 10$ arises from the long-range nature of gravity. The parameter $p \approx \frac{1}{2}$ corresponds to the fraction of DM particles moving slower than v_{rel} , and both parameters carry moderate astrophysical uncertainties.

In our case, where the BH gravity dominates, the relative velocity v_{rel} between the approaching SMBH and the ULDM particles (i.e. into the soliton core) is comparable to the orbital speed of SMBH i.e. $v_{rel} \approx \omega r$ if the SMBH mass is $\lesssim 10^{9.5} M_{\odot}$ and for ULDM mass $\sim 10^{-21} \text{eV}$ in the nHz frequencies. With these into consideration, the energy dissipation due to this dynamical friction is

$$\mathcal{W}_{DF} = F_{DF} v_{rel} = \frac{4\pi G_N^2 \mu^2 \rho}{\omega r} C_{cl}(\Lambda), \quad (26)$$

The GW spectrum is characterized by the dimensionless strain h_c , related to the GW energy density Ω_{GW} as[44]

$$\begin{aligned} \rho_c \Omega_{GW}(f) &= \frac{\pi}{4G_N} f^2 h_c^2(f) \\ &= \int \frac{dz}{1+z} \int dX \frac{dn_s}{dzdX} \left(f_s \frac{dE_{GW}}{df_s} \right) \Bigg|_{f_s=f(1+z)} \end{aligned} \quad (27)$$

where $dn_s/dz dX$ is the number of merger events per unit comoving volume between redshifts z and $z + dz$. X collectively denotes all SMBH sources distributed over that redshifts. Computation related to the SMBH merger rate are given in the Appendix C. The f_s denotes the GW frequency at the source and f signifies the observed frequency when the merger occurs at the redshift z from earth.

The strain can be expressed as a power law:

$$h_c^2(f) = \left[A_{GW} \left(\frac{f}{f_{ref}} \right)^\beta \right]^2 \quad (28)$$

Here, $\rho_c = 3H_0^2/8\pi G_N$ is the critical density of the universe, and A_{GW} is the amplitude and f_{ref} is the reference frequency at which the PTA measurements provide best accuracy.

Including energy losses from ULDM dynamical friction and GW emission, the GW energy spectrum is[75]:

$$\frac{dE_{GW}}{df_s} = \frac{\mu}{3} \left[\pi G_N (M_1 + M_2) \right]^{2/3} f_s^{-1/3} \frac{1}{1 + \frac{\mathcal{W}_{DF}}{\mathcal{W}_{GW}}} \quad (29)$$

The density ρ is determined using the soliton density profiles outlined in Section II B. We assume the mass ratio of the merging SMBHs is q_\bullet , such that $M_1 + M_2 = M_\bullet(1 + q_\bullet)$, where $M_1 \equiv M_\bullet$ and $q_\bullet \lesssim 1$ in this analysis. Now we identify the distance scale at which the dynamical friction becomes the dominant energy loss mechanism. We define the critical radius r_{cr} of the soliton core as the distance where the two dissipative forces are equal, i.e., $\mathcal{W}_{GW} = \mathcal{W}_{DF}$. Assuming the central soliton density $\rho_0 = \rho(r=0)$, the critical radius is expressed as:

$$r_{cr} = \sqrt[11]{\frac{64G_N^5 M_\bullet^7 (1 + q_\bullet)^7}{25\pi^2 \rho_0^2 C_{cl}^2}} \quad (30)$$

This expression depends on the soliton density, which itself is a function of the ULDM mass, the self-coupling parameter λ , and the mass of the merging SMBH. For a benchmark case where $M_\bullet = 10^{8.5} M_\odot$, $m = 10^{-21} \text{eV}$ and dimensionless self coupling $\hat{\lambda}_{in} = -1.0$, the critical radius evaluates to approximately $8 \times 10^{-3} \text{pc}$. Using Kepler's law, the corresponding radial frequency f_{cr} is 3.72nHz, well within the detection range of current PTA

experiments. Putting the loss powers \mathcal{W}_{GW} and \mathcal{W}_{DF} , we get the frequency spectra,

$$\frac{dE_{GW}}{df_s} = \frac{\pi^{2/3} q_\bullet G_N^{2/3} M_\bullet^{5/3} f_s^{-1/3}}{3(1 + q_\bullet)^{1/3}} \frac{1}{1 + \left(\frac{f_{cr}}{f_s} \right)^{11/3} e^{-\left(\frac{f_{sol}}{f_s} \right)^{2/3}}} \quad (31)$$

From the above expression, it is evident that in the absence of \mathcal{W}_{DF} , the energy loss follows the standard power-law behavior, $dE_{GW}/df_s \propto f_s^{-1/3}$. However, the presence of dynamical friction, influenced by the soliton dark matter density, distorts the strain amplitude. The radial frequency f_{sol} corresponds to the soliton radius r_{sol} of the dark matter density. When $f_{cr} < f_{sol}$, i.e. the critical radius greater than the soliton radius the energy loss due to GW emission is prominent than the dynamical friction. In this case the spectrum follow the standard power law behaviour. On the other hand, when the critical radius is inside the soliton core ($f_{cr} > f_{sol}$), the dynamical friction is dominant and the frequency spectrum follows completely different frequency dependence. Due to the soliton core made of the ULDM, the strain of the spectrum shows sudden dip. In certain cases when the two frequencies are very close to each other, the dip in the amplitude is even higher indicating a resonance phenomenon.

IV. RESULTS

A. The GW spectrum

Using Eq. 27 and substituting the energy loss power from Eq. 31, we derive the strain of GW. The soliton density profile influences this spectrum through dynamical friction, as discussed in the previous section. The strains are shown in Fig. 2 for the merging SMBH masses $10^{8.5} M_\odot$ and in Fig. 3 for merging SMBH masses $10^9 M_\odot$. The cases for two ULDM masses are shown in sub-figures.

In the absence of self-interactions among ULDM particles, represented by $\hat{\lambda} = 0$, the GW spectrum follows the black dotted line. Non-zero values of $\hat{\lambda}$, which denote self-interactions, modify the spectrum. Specifically, positive $\hat{\lambda}$, corresponding to repulsive soliton cores, are depicted with solid lines, while negative $\hat{\lambda}$, representing attractive soliton cores, are shown with dashed lines. If GWs are generated purely by mergers without incorporating the effects of dynamical friction (i.e., ignoring dark matter densities), the GW strain follows a simple power-law behavior ($h_c \propto f^{-2/3}$), represented by the black dashed line. The slope of the spectrum deviates from this power-law due to the influence of dark matter density, where the soliton serves as the dark matter profile in this analysis.

The PTA experiments operate in the frequency range of 1–30 nHz and can probe features of the ULDM, such as self-interactions. Within this window, PTA observations can constrain the value of $\hat{\lambda}$, providing a dimensional

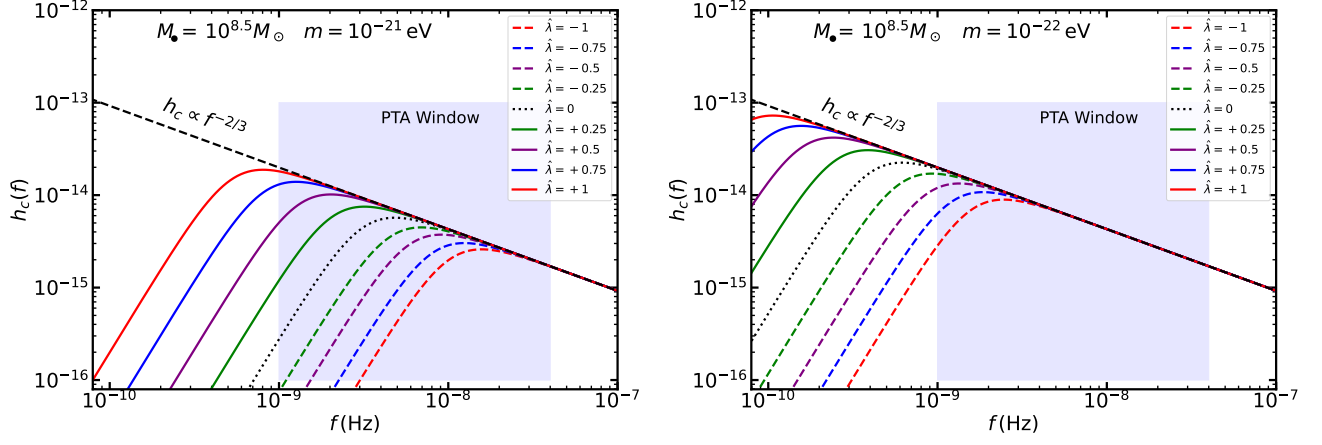


FIG. 2: The GW strains corresponding to different DM density profiles, characterized by distinct self-coupling parameters, are displayed. (Left) For a ULDM mass of 10^{-21} eV and an SMBH mass of $10^{8.5} M_\odot$ of the binary, the strains associated with varying $\hat{\lambda}$ parameters are shown, exhibiting deviations from the power-law behavior ($h_c \propto f^{-2/3}$). (Right) The strains are presented for a ULDM mass of 10^{-22} eV. The blue-shaded region represents the PTA observation window for the SGWB generated by black hole mergers in a solitonic dark matter environment with self-interacting ULDM particles.

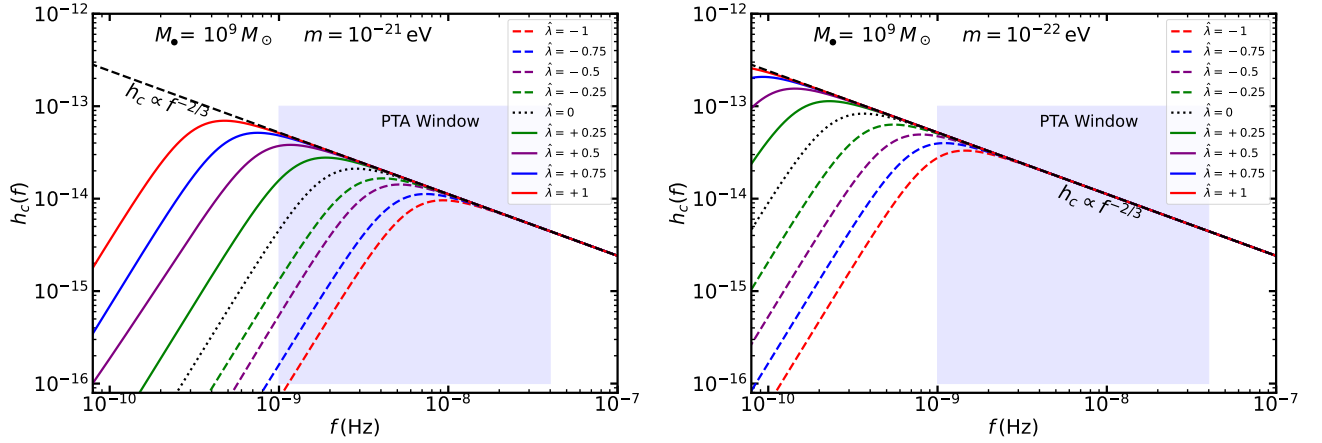


FIG. 3: The GW strains corresponding to different DM density profiles, characterized by distinct self-coupling parameters, are displayed. (Left) For a ULDM mass of 10^{-21} eV and an SMBH mass of $10^9 M_\odot$ of the binary, the strains associated with varying $\hat{\lambda}$ parameters are shown, demonstrating deviations from the power-law behavior ($h_c \propto f^{-2/3}$). (Right) The strains are shown for a ULDM mass of 10^{-22} eV. The blue-shaded region marks the PTA observation window for the SGWB.

estimate of the self-interaction strength. This constraint would carry characteristic signatures detectable through the GW spectrum.

B. Typical values of self coupling $\hat{\lambda}$

The interplay between the strength of gravity and the self-interaction of ULDM particles plays a crucial role in the formation of soliton cores. From the GPP equations, the ratio of the gravitational potential energy, $m\Phi\Psi$, to

the self-interaction energy, $\frac{\lambda}{8m^3}|\Psi|^3$, is given by:

$$\frac{\text{gravity}}{\text{self interaction}} = \frac{8m^4\Phi}{\lambda|\Psi|^2} = \frac{4}{\lambda} \left(\frac{M_{\text{pl}}}{m}\right)^{-2} \left(\frac{L}{m^{-1}}\right)^2, \quad (32)$$

L being the physical size of the soliton. This shows that gravity becomes more significant than self-interactions as the soliton size increases. Using the definition of the dimensionless self-coupling parameter $\hat{\lambda}$, this ratio can be rewritten as:

$$\frac{\text{gravity}}{\text{self interaction}} = \frac{1}{2\hat{\lambda}}. \quad (33)$$

For gravity to dominate over self-interactions, we require:

$$-\frac{1}{2} \leq \hat{\lambda} \leq \frac{1}{2}. \quad (34)$$

Here, a negative $\hat{\lambda}$ corresponds to attractive self-interactions, while a positive $\hat{\lambda}$ corresponds to repulsive self-interactions. In this study, we do not focus on cases where self-interactions dominate gravity, as the GPP equations enter into a highly non-linear regime, introducing additional complexities.

Eq. 34 gives a dimensionless limit of the self-coupling parameter $\hat{\lambda}$, as long as gravity dominates over the self interaction of ULDM particles and that the soliton cores at the galactic centers remain stable.

C. Imposing limits on λ

The typical frequency range probed by PTA experiments for the SGWB spans the 1–30 nHz window. Within this range, a sudden dip in the strain spectrum can provide constraints on the self-coupling parameter $\hat{\lambda}$, which in turn determines the dimensionful coupling strength λ . For a black hole mass of $10^{8.5}M_{\odot}$ in the equal mass binary, the attractive self-coupling values (0 to -1) fall within the observation window for an ULDM mass of 10^{-21} eV. However, for lighter ULDM masses, the peak of the spectrum shifts to lower frequencies, and only the negative $\hat{\lambda}$ values remain within the window.

As discussed previously, the maximum allowed value for $\hat{\lambda}$ is limited to ± 0.5 , which restricts the ability to constrain the coupling through the SGWB. From Eq. 10, the strength of the coupling for a ULDM mass of 10^{-21} eV is approximately $\mathcal{O}(10^{-96})$ for both attractive and repulsive self-couplings. The $\hat{\lambda}$ parameter scales with the s^2 factor, increasing the coupling strength by several orders of magnitude. For instance, for a ULDM mass of 10^{-21} eV and $\hat{\lambda} = -0.5$, the coupling strength λ increases to approximately -3.47×10^{-92} . Similarly, for a ULDM mass of 10^{-22} eV and $\hat{\lambda} = -0.5$, λ is approximately -1.23×10^{-93} .

As the scaling s increases, the strength of λ grows even larger for positive $\hat{\lambda}$ values. However, repulsive self-coupling ($+\hat{\lambda}$) marginally falls within the observational window for a ULDM mass of 10^{-21} eV, while for lighter ULDM masses, the repulsive coupling parameters shift outside the window. For higher black hole masses of the binary populations, the amplitude of the SGWB changes without affecting the spectral slope.

For large strengths of attractive self-interactions, the balance between gravity, self-interactions, and quantum pressure cannot be maintained, resulting in the absence of stable soliton solutions. A stable soliton exists only up to a maximum possible soliton mass, M_c , given by [77, 78]:

$$M_c \approx 10.2 \frac{M_{\text{pl}}}{(-\lambda)^{1/2}} \quad (35)$$

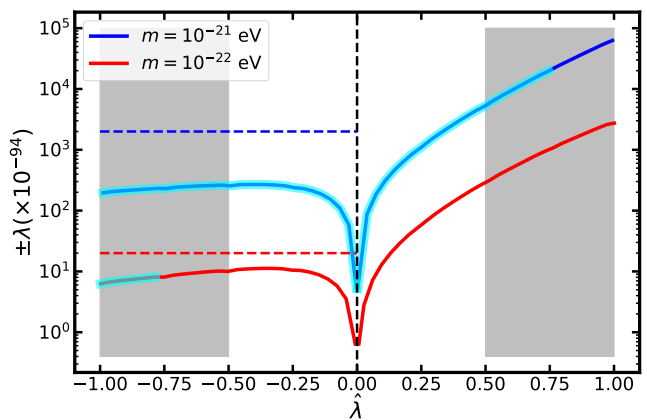


FIG. 4: The estimated values of the λ parameter are shown along with the dimensionless $\hat{\lambda}$, considering both positive and negative values (-ve estimate of λ is for the -ve values of the $\hat{\lambda}$ and positive λ is for the positive $\hat{\lambda}$ values). The plots are presented for two different ULDM masses but keeping the SMBH mass to $10^{8.5}M_{\odot}$. The cyan shading over the plots represents the range that can be probed through PTA observations, while the gray shaded region indicates the excluded region for the $\hat{\lambda}$ parameter based on theoretical considerations discussed in Section. IV B. Dashed lines (blue and red), corresponding to the attractive self-coupling parameters derived using Eq. 36, illustrate the upper limit on the strength of λ .

where the negative sign indicates an attractive self-interaction. For a galaxy with a mass $M_{\text{halo}} = 10^{13}M_{\odot}$, the soliton mass can be determined using Eq. 13 and then incorporating an appropriate scaling. From this, an upper limit is established to ensure the soliton mass does not exceed M_c , given by:

$$|-\lambda| \leq 1.77 \times 10^{-91} \left(\frac{m}{10^{-21}} \right)^2 \quad (36)$$

In Fig. 4, the maximum possible coupling is represented by dashed lines corresponding to different masses of ULDM and SMBH mass of $10^{8.5}M_{\odot}$ in binary populations having equal masses. The cyan shading over the blue and red plots delineates the range of self-coupling limits which can be probed from the SGWB spectrum amplitude.

D. Relation between the GW amplitude and the γ_{GW} parameter

PTAs probe the SGWB generated by SMBH mergers in the nHz frequency range. The PTA data analyzes the strain spectrum, typically parameterized as a power law: $h_c(f) = A_{\text{GW}}(f/f_{\text{PTA}})^{\beta}$ where f_{PTA} is a reference

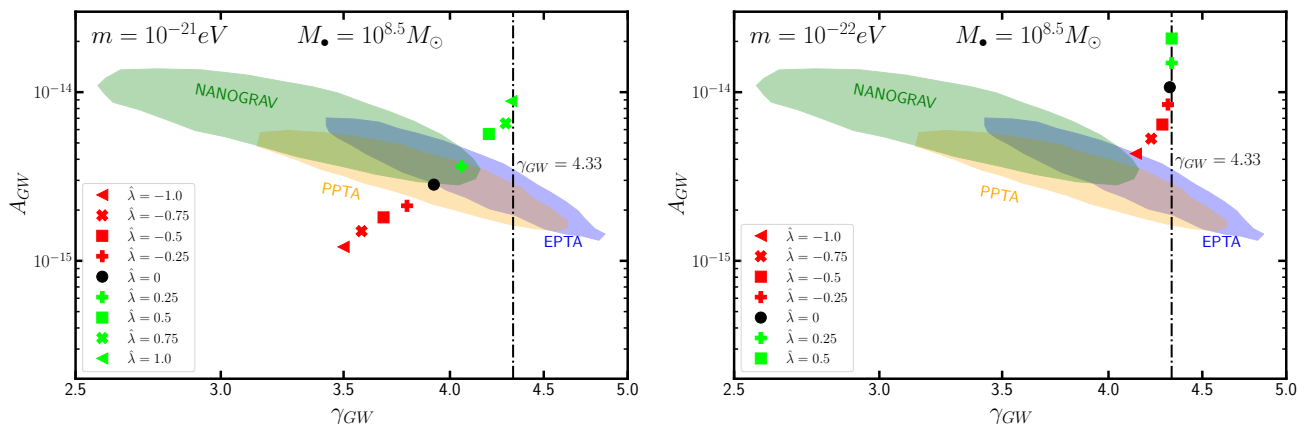


FIG. 5: The amplitude of the GW strain with change of γ_{GW} parameter for PTA observations by NANOGrAV, EPTA, and PPTA are represented by the shaded regions[76] within 2σ confidence interval for the GW signal. For a reference frequency (f_{PTA}) of 1 nHz, the amplitude and γ_{GW} values corresponding to different $\hat{\lambda}$ parameters are depicted using various legends. For a equal mass non-eccentric binary systems, keeping the SMBH mass fixed at $10^{8.5} M_{\odot}$, the correlation between A_{GW} and γ_{GW} for a ULDM mass of 10^{-21} eV is shown in the left figure, while for a ULDM mass of 10^{-22} eV, it is displayed in the right figure. The dashed vertical line at the $\gamma_{GW} = 4.33$ is the corresponding value for a GW strain that exactly follows the power-law $h_c \propto f^{-2/3}$.

frequency. The GW spectrum is characterized by the amplitude A_{GW} and the slope parameter $\gamma_{GW} = 3 - 2\beta$.

Astrophysical environments in the vicinity of SMBHs can alter the spectral slope, causing it to deviate from that expected solely from gravitational wave radiation losses. Our focus is on the scenario where dynamical friction between SMBHs and the ULDM environment is the dominant energy dissipation process. In circular binaries driven primarily by GW radiation losses, the spectral index is $\beta = -2/3$, corresponding to $\gamma_{GW} = 13/3$. However, if dynamical friction dominates, deviations in γ_{GW} arise, providing a pathway to constrain the self-coupling parameter of ULDM.

Tentative SGWB signal found at frequencies above 1 nHz as fit by NANOGrav, EPTA, and PPTA often expressed through correlation of the GW amplitude A_{GW} and the γ_{GW} parameter[76]. So we set the reference frequency at $f_{PTA} = 1$ nHz for this analysis.

The Fig. 5 describes the relation between the GW amplitude and the slope parameter γ_{GW} for the two cases : the left one is for ULDM mass $m = 10^{-21}$ eV and the right one is for $m = 10^{-22}$ eV and keeping the SMBH mass fixed at $10^{8.5} M_{\odot}$. The effect of the self-coupling which are specified by different legends are shown in the figures. As depicted, the range of the $\hat{\lambda}$ parameter that lies within the correlated regions defined by the current PTA observations is relatively narrow. The cases for SMBH mass $10^9 M_{\odot}$ has been stacked in the Appendix D with the present case for comparison.

E. Probing self coupling of Ultralight Axions

Axion or Axion-Like Particle(ALP) can also serve as ULDM and form the solitonic cores[20]. In this case the relic abundance of dark matter is set by the initial misalignment angle of the cosine potential,

$$U(\phi) = m_a^2 f^2 \left(1 - \cos\left(\frac{\phi}{f}\right) \right) \quad (37)$$

where, f is the decay constant of the axion or ALP and using this potential, the quartic self coupling shall be given by $\lambda_a = -(m_a/f)^2$. For axions with $f \sim \mathcal{O}(10^{16})$ GeV and $m_a \sim 10^{-21}$ eV (extremely light or ULA) one gets the self coupling $\lambda_a \sim -10^{-92}$. If the axions possess all of the DM content, the corresponding relic density is given by[24] $\Omega_a \sim 0.1 \left(\frac{m}{10^{-21} \text{eV}}\right)^{1/2} \left(\frac{f}{10^{16} \text{GeV}}\right)^2$ which again imply that $\Omega_a \sim 0.1 \left(\frac{m}{10^{-21} \text{eV}}\right)^{5/2} \left(\frac{10^{-92}}{-\lambda}\right)$. Only the attractive self coupling for ULAs can be probed using the SGWB spectrum but the repulsive coupling is forbidden through the nature of the cosine potential.

V. DISCUSSION AND CONCLUSION

In this study, we have explored the possibility of putting constraints on the ULDM self-coupling λ using the recent PTA observation. The ULDM with masses $\sim (10^{-22} - 10^{-20})$ eV, can form dense cores at the centers of the galaxies, known as solitons. The merger of black holes within the dense dark matter environments such as these soliton cores can impact the stochastic gravitational wave background. The presence of the self interac-

tion of the ULDM particles would modify the GW strain through dynamical friction. We have inspected which part of the SMBH population can contribute to the GW signal. For non-eccentric equal mass SMBH binaries, the SMBH masses around $\sim 10^{8.5}M_{\odot}$ mostly contribute to the strain h_c at the nano hertz frequencies of the spectrum.

The empirical relations of the soliton mass and central SMBH mass infer that the GPP equation solved numerically for the DM halo mass $\sim 10^{13}M_{\odot}$ would give the best results on the GW spectrum. We numerically solve the GPP equations by fixing the central black hole parameter α , adopted from Ref. [50], corresponding to a halo mass of $10^{13}M_{\odot}$. This value is based on simulations where the central supermassive black hole (SMBH) is treated as a point mass embedded in a virialized halo. For each solution, the self-coupling parameter λ is also fixed, as shown in Fig. 6 (presented in Appendix A). The corresponding dark matter densities are then obtained by applying the appropriate scaling to convert the results into physical units. The presence of self coupling λ with characteristic signature will change the DM profiles as shown in Fig. 1. These individual ULDM density profiles (through the solitonic core formation) leads to various GW strains, which are presented in Fig. 2 and Fig. 3 corresponds to different self-coupling parameter λ .

The nanohertz window of the spectrum is particularly sensitive to recent observations from EPTA, PPTA, and NANOGrav. Deviations in the strain caused by the λ parameter from the usual power-law dependence ($h_c \propto f^{-2/3}$) can help identify the range and characteristic signature of λ that falls within this frequency band. Based on this analysis, we can place constraints on λ for specific ULDM masses, as shown in Fig. 4 for a fixed SMBH mass. Our results indicate that attractive self-coupling ($\lambda < 0$) can be best probed through GW strains when ULDM masses are in the range $\sim (5 \times 10^{-22} - 10^{-21})$ eV, given an SMBH mass of $10^{8.5}M_{\odot}$. In contrast, repulsive self-coupling ($\lambda > 0$) can be probed within a specific range of the dimensionless $\hat{\lambda}$ parameter for ULDM masses around $\sim 10^{-21}$ eV. The soliton cores made out of the ULDM particles with masses exceeding $\gtrsim 10^{-21}$ eV, are excluded due to accretion time constraints caused by the gravitational attraction of central SMBHs in galaxies. Therefore, accounting for the self-coupling effects of ULDM particles requires precise tuning of both the ULDM mass and the masses of the merging SMBHs.

If ultralight axions (ULAs) constitute the entire dark matter component of the universe and undergo soliton core formation in galactic centers, their self-coupling parameter is approximately $\mathcal{O}(10^{-92})$ for masses around $\sim 10^{-21}$ eV.

Our study focuses on probing self-interactions, particularly in the context of solitonic core formation, through the GWB spectrum rather than conducting a detailed PTA data analysis. Advanced data-driven techniques can be employed in the future for a more thorough investigation.

Upcoming PTA experiments, such as IPTA30 [79], are expected to reach frequencies up to $\mathcal{O}(100)$ nHz and analyze SMBH populations with masses as low as $M_{\bullet} \simeq 10^6M_{\odot}$ [80], providing a more rigorous probe of self-interactions of ULDM particles. In addition to PTA detection of GWs from SMBHs orbiting soliton cores, the planned LISA mission, operating in the milli-hertz frequency band, may also provide detection capabilities [81].

ACKNOWLEDGMENTS

We sincerely thank Soumitra SenGupta, Satyanarayan Mukhopadhyay, and Sumanta Chakraborty for engaging discussions. In particular, we are indebted to Sumanta Chakraborty for his detailed and constructive feedback on the manuscript. We also thank Sourov Roy for carefully going through the draft and offering helpful suggestions. The author acknowledges financial support from the University Grants Commission, Government of India, as a Senior Research Fellow

Appendix A: Numerically produced solutions of Gross-Pitaevskii-Poisson equation

The Gross-Pitaevskii-Poisson equation in dimensionless form is given by

$$\frac{1}{2}\hat{\nabla}^2 = \left(\hat{V} - \hat{\gamma} - \frac{\hat{\alpha}}{\hat{r}} + 2\hat{\lambda}\hat{\chi}^2 \right) \hat{\chi} \quad (\text{A1})$$

$$\hat{\nabla}^2 \hat{V} = \hat{\chi}^2 \quad (\text{A2})$$

with the boundary conditions: $\hat{\chi}(\hat{r} = \infty) = 0, \hat{\chi}'(\hat{r} =$

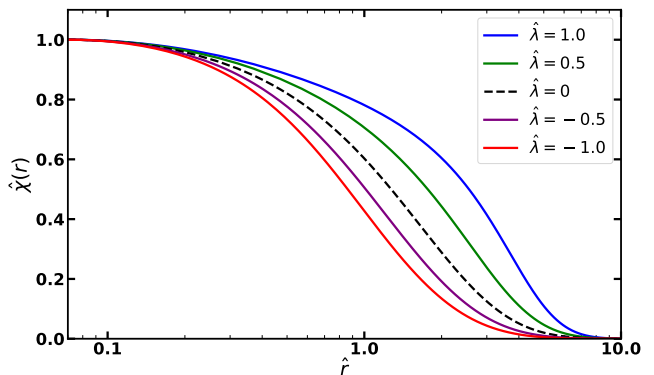


FIG. 6: Solutions of the coupled, dimensionless Gross-Pitaevskii-Poisson equation A1 for various values of $\hat{\lambda}$ keeping $\hat{\alpha}$ fixed at 0.48 for a ULDM mass of 10^{-21} eV.

$0) = 0, \hat{V}(\hat{r} = 0) = 0, \hat{V}'(\hat{r} = 0) = 0$. We use the arbitrary normalization $\hat{\chi}(\hat{r} = 0) = 1$ to get the non zero value at the center. For a fixed SMBH mass parameter $\hat{\alpha}$ corresponding to halo mass $M_{halo} = 10^{13}M_{\odot}$ (shown in

the table), we choose the $\hat{\lambda}$ parameter of $\mathcal{O}(1)$. To solve this system of differential equations, we apply a shooting method. This method integrates the solution from $\hat{r} = 0$, aiming to satisfy the asymptotic boundary condition $\hat{\chi}(\hat{r} = \infty) = 0$. To achieve this, an initial guess for $\hat{\gamma}$ is needed, as only quantized values meet the asymptotic boundary conditions. Using a standard root-finding technique, we determine the smallest $\hat{\gamma}_0$ that satisfies the boundary conditions, giving the 0-node (ground state) solution. Figure 6 illustrates the dimensionless solutions obtained for various values of $\hat{\lambda}$ with a specific $\hat{\alpha}$ value. In the limit of large $\hat{\alpha}$ (representing a large black hole mass), the solution approaches the exponential form characteristic of the hydrogen atom. As with the previous variables we define a dimensionless mass:

$$\hat{M} \equiv \frac{GMm}{\hbar c} = \int_0^\infty \hat{\chi}^2 \hat{r}^2 d\hat{r}. \quad (\text{A3})$$

A relevant parameter in our analysis is the ratio of the soliton mass to the black hole mass. To ensure that the SMBH acts as the dominant perturbing potential in the system, this ratio has been kept at $\lesssim 0.3$ throughout the study[50], allowing us to recover the exponential solutions.

Appendix B: Amount of scaling s

Fixing the halo mass, M_{halo} , there exists an empirical relationship between soliton mass M_{sol} and halo mass[69]:

$$M_{\text{sol}} = 1.25 \times 10^9 \left(\frac{M_{\text{halo}}}{10^{12} M_\odot} \right)^{1/3} \left(\frac{m}{10^{-22} \text{ eV}} \right)^{-1} M_\odot. \quad (\text{B1})$$

This relation is derived from DM-only simulations without SMBHs and is valid for $M_{\text{halo}} \sim (10^9 - 5 \times 10^{11}) M_\odot$. For $M_{\text{halo}} \gtrsim 10^{12} M_\odot$ or different ULDM mass values, the relation weakens but remains useful for our goal of constraining the self-coupling parameter via the SGWB.

In this work, we assume $M_{\text{halo}} = 10^{13} M_\odot$ and use the $\hat{\alpha}$ values from [50] to construct density profiles. These values of $\hat{\alpha}$ obtained using numerical simulation considering virialized halo with SMBH placed at the centers of the galaxies. Table I summarizes $\hat{\alpha}$ and the corresponding dimensionless soliton mass \hat{M} for different ULDM masses:

With fixed $\hat{\alpha}$ and nonzero $\hat{\lambda}$, we compute \hat{M} . For attractive self-interaction ($\hat{\lambda} < 0$) and repulsive ($\hat{\lambda} > 0$), \hat{M} relates to M_{sol} by:

$$\hat{M} \equiv \frac{G_N M_{\text{sol}} m}{\hbar c}. \quad (\text{B2})$$

Scaling modifies \hat{M} as:

$$\hat{M} \rightarrow \frac{1}{s} \hat{M} \quad (\text{B3})$$

M_{halo}	m (eV)	$\hat{\alpha}$	\hat{M}
$10^{13} M_\odot$	10^{-22}	0.10	1.77
$10^{13} M_\odot$	5×10^{-22}	0.28	1.35
$10^{13} M_\odot$	10^{-21}	0.48	0.84

TABLE I: Values of $\hat{\alpha}$ chosen to produce density profiles of halo mass $10^{13} M_\odot$ without the λ parameter, along with the dimensionless soliton mass \hat{M} for different ULDM masses.

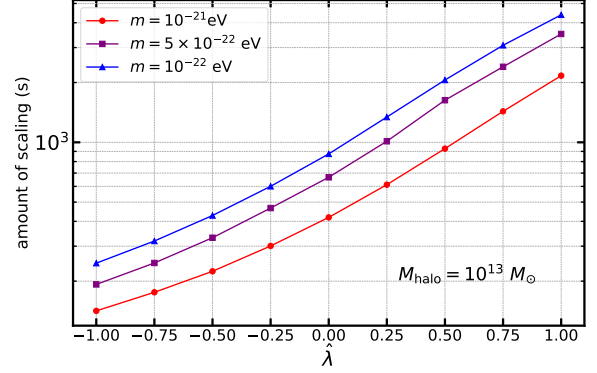


FIG. 7: Amount of scaling with different values of $\hat{\lambda}$ parameter for a fixed halo mass. Three cases are shown for three ULDM masses.

Using the relations above, we calculate the scaling factor s :

$$s = \frac{1.33 \times 10^{12}}{1.25 \times 10^9} \left(\frac{M_{\text{halo}}}{10^{12} M_\odot} \right)^{-1/3} \hat{M}. \quad (\text{B4})$$

The dimensionless soliton mass \hat{M} is calculated numerically through the integral A3 for each soliton solutions with the non zero $\hat{\lambda}$ parameters.

Figure 7 illustrates how s changes with $\hat{\lambda}$. The scaling s increases with decreasing ULDM mass for a fixed $\hat{\lambda}$, and s also grows as $\hat{\lambda}$ shifts from negative to positive values.

Appendix C: SMBH binary merger rate

Here we will shortly describe the parameters needed to calculate the number of merger events between SMBH binaries from the galaxy merger rate, available in the literature[46, 82–85]. As detailed in [85], the differential galaxy merger rate per unit redshift, mass and mass ratio, can be written as,

$$\frac{d^3 n_G}{dz dM_G dq} = \frac{\phi(M_G, z) \Upsilon(M_G, z, q)}{M_G \log 10 \tau(M_G, z, q)} \frac{dt}{dz} \quad (\text{C1})$$

where $\phi(M_G, z)$ is galaxy stellar mass function(GSMF), $\Upsilon(M_G, z, q)$ is the differential pair function and $\tau(M_G, z, q)$ is the merger timescale. Here M_G is the primary galaxy mass, q is the mass ratio of galaxy pair and

z is the redshift of the galaxy pair. This galaxy merger

rate can be converted into the SMBH binary merger rate through

$$\frac{dn_s}{dzdX} \equiv \frac{d^3n}{dzdM_{BH}dq_{BH}} = \frac{d^3n_G}{dzdM_Gdq} \frac{dM_G}{dM_{BH}} \frac{dq}{dq_{BH}} \quad (\text{C2})$$

The galaxy stellar masses needs to be translated into SMBH masses. The total mass of a galaxy M_G can be

converted into its bulge mass M_{bulge} using phenomenological fitting function [83, 86],

$$\frac{M_{bulge}}{M_G} = \begin{cases} \frac{\sqrt{6.9}}{(\log M_G - 10)^{1.5}} \exp\left(\frac{-3.45}{\log M_G - 10}\right) + 0.615, & \text{if } \log M_G > 10, \\ 0.615, & \text{if } \log M_G \leq 10. \end{cases} \quad (\text{C3})$$

Now according to [55] the scaling between the galaxy bulge mass M_{bulge} and black hole mass M_{BH} is of the form

$$\log_{10} \left(\frac{M_{BH}}{M_\odot} \right) = \mu + \alpha_* \log_{10} \left(\frac{M_{bulge}}{10^{11} M_\odot} \right) + \mathcal{N}(0, \epsilon) \quad (\text{C4})$$

Here \mathcal{N} is the normal distribution with mean 0 and standard deviation ϵ , to translate galaxy mass into BH mass. The black hole mass ratio q_{BH} is related to galaxy mass ratio q through $q_{BH} = q^{\alpha_*}$. The galaxy stellar mass function written as

$$\phi(M_G, z) = 10^{\phi_0 + \phi_I z} \left(\frac{M_G}{M_0} \right)^{1 + \alpha_0 + \alpha_I z} \exp\left(\frac{-M_G}{M_0}\right) \ln 10 \quad (\text{C5})$$

The five parameters $\phi_0, \phi_I, M_0, \alpha_0, \alpha_I$ are sufficient to describe the GSMF. The differential galaxy pair function is given by,

$$\Upsilon(M_G M_G, z, q) = f'_0 \left(\frac{M_G}{10^{11} M_\odot} \right)^{\alpha_f} (1+z)^{\beta_f} q^{\gamma_f} \quad (\text{C6})$$

The quantity f_0 is related to f'_0 through $f_0 = f'_0 \int q^{\gamma_f} dq$. So there are four model parameters $f'_0, \alpha_f, \beta_f, \gamma_f$. The merger timescale written as,

$$\tau(M_G, z, q) = \tau_0 \left(\frac{h_0 \times M_G}{0.4 \times 10^{11} M_\odot} \right)^{\alpha_\tau} (1+z)^{\beta_\tau} q^{\gamma_\tau} \quad (\text{C7})$$

Here, $\tau_0, \alpha_\tau, \beta_\tau, \gamma_\tau$ are another four model parameters. The quantity $\frac{dt}{dz}$ is given assuming a flat Lambda CDM

model as,

$$\frac{dt}{dz} = \frac{1}{H_0(1+z)\sqrt{\Omega_M(1+z)^3 + \Omega_k(1+z)^2 + \Omega_\Lambda}} \quad (\text{C8})$$

Here, Hubble parameter is $h_0 = 0.7$ and Hubble constant $H_0 = 70 \text{ kmMpc}^{-1}\text{s}^{-1}$ and energy density ratios $\Omega_M = 0.3, \Omega_k = 0$, and $\Omega_\Lambda = 0.7$.

Summarizing, the SMBH binary merger rate is described using 18 empirical parameters that are estimated through astrophysical observations (See [85] for details). The SGWB signal is most sensitive for primary black-hole masses in between $10^8 M_\odot$ and $10^9 M_\odot$ and redshift parameter $z \lesssim 0.3$. The SMBH binary merger rate is typically estimated using the Holodeck library [38].

Appendix D: Plots of GW-strain amplitude vs γ_{GW} parameter space

An alternative way to analyze the self-coupling of ULDM is through the correlation between the GW amplitude, A_{GW} and the slope parameter of the GW, γ_{GW} . As discussed in [76], recent PTA observations reveal a correlation between these parameters, represented by the shaded regions in Fig. 8. Overlaid on these regions are data points derived from GW strains corresponding to solitonic profiles with different λ values. The figures indicate that self-coupling is most effectively probed for a ULDM mass of $\sim 10^{-21} \text{ eV}$, whereas for lighter masses, the signal shifts beyond the correlated regions detectable by current PTA observations. Additionally, for an SMBH of mass $10^9 M_\odot$, the strain amplitude increases compared to that for an SMBH of $10^{8.5} M_\odot$, consistent with merger calculations. The vertical dot-dashed line represents the value of γ_{GW} in the absence of a DM environment around the SMBH merger, where the GW strain follows the expected power-law behavior $h_c \propto f^{-2/3}$.

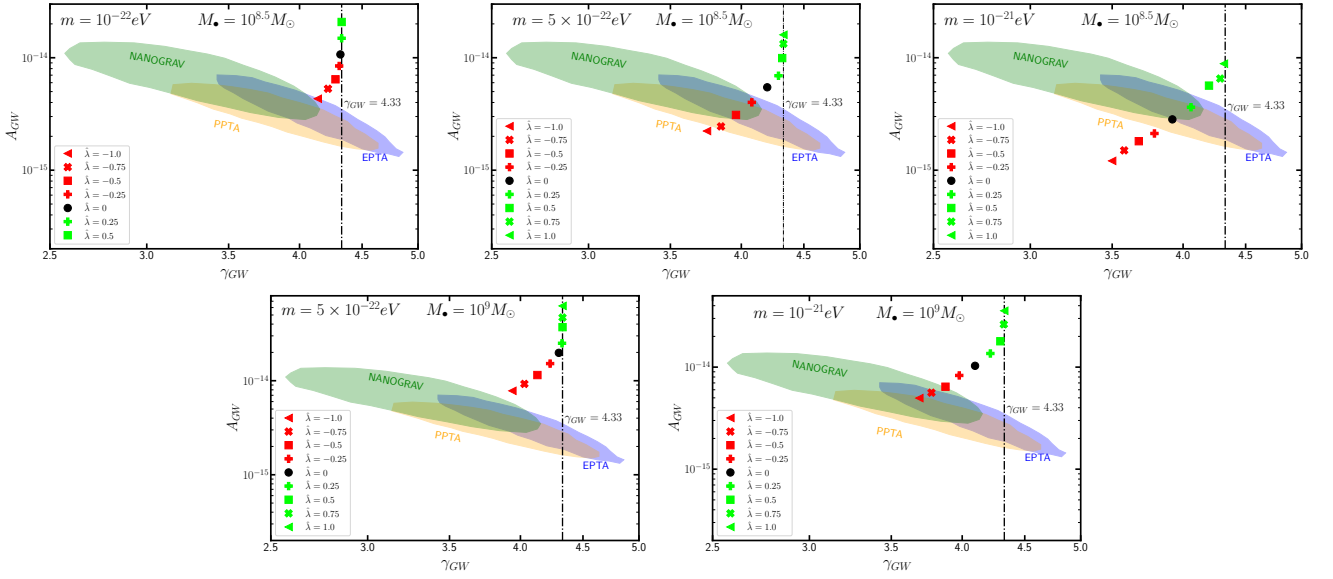


FIG. 8: Correlation between the GW amplitude (A_{GW}) and the GW slope parameter (γ_{GW}) for different UDM self-coupling parameters. The shaded regions represent the correlation observed in recent PTA data [76] within 2σ confidence level for a GW signal. The overlaid points correspond to GW strains derived from solitonic profiles with varying λ parameters. The top panel shows results for a equal mass binary populations where each SMBH has a mass of $10^{8.5}M_{\odot}$, while the bottom panel corresponds to each SMBH having a mass of 10^9M_{\odot} . The vertical dot-dashed line represents the value of γ_{GW} , where the GW strain follows the power-law relation $h_c \propto f^{-2/3}$. The reference frequency f_{ref} is taken to be 1 nHz in Eq. 28 to estimate the correlated data points corresponding to different strains of solitonic density profiles.

- [1] V. C. Rubin, N. Thonnard, and W. K. Ford, Jr., Rotational properties of 21 SC galaxies with a large range of luminosities and radii, from NGC 4605 / $R = 4\text{kpc}/$ to UGC 2885 / $R = 122\text{kpc}/$, *Astrophys. J.* **238**, 471 (1980).
- [2] E. Corbelli and P. Salucci, The Extended Rotation Curve and the Dark Matter Halo of M33, *Mon. Not. Roy. Astron. Soc.* **311**, 441 (2000), arXiv:astro-ph/9909252.
- [3] A. Refregier, Weak gravitational lensing by large scale structure, *Ann. Rev. Astron. Astrophys.* **41**, 645 (2003), arXiv:astro-ph/0307212.
- [4] S. W. Allen, A. E. Evrard, and A. B. Mantz, Cosmological Parameters from Observations of Galaxy Clusters, *Ann. Rev. Astron. Astrophys.* **49**, 409 (2011), arXiv:1103.4829 [astro-ph.CO].
- [5] V. A. Rubakov, Cosmology and dark matter, *CERN Yellow Rep. School Proc.* **5**, 129 (2022), arXiv:1912.04727 [hep-ph].
- [6] N. Aghanim *et al.* (Planck), Planck 2018 results. VI. Cosmological parameters, *Astron. Astrophys.* **641**, A6 (2020), [Erratum: *Astron. Astrophys.* 652, C4 (2021)], arXiv:1807.06209 [astro-ph.CO].
- [7] S. Profumo, L. Giani, and O. F. Piattella, An Introduction to Particle Dark Matter, *Universe* **5**, 213 (2019), arXiv:1910.05610 [hep-ph].
- [8] G. Bertone and D. Hooper, History of dark matter, *Rev. Mod. Phys.* **90**, 045002 (2018), arXiv:1605.04909 [astro-ph.CO].
- [9] P. W. Graham, I. G. Irastorza, S. K. Lamoreaux, A. Lindner, and K. A. van Bibber, Experimental Searches for the Axion and Axion-Like Particles, *Ann. Rev. Nucl. Part. Sci.* **65**, 485 (2015), arXiv:1602.00039 [hep-ex].
- [10] M. Schumann, Direct Detection of WIMP Dark Matter: Concepts and Status, *J. Phys. G* **46**, 103003 (2019), arXiv:1903.03026 [astro-ph.CO].
- [11] J. M. Gaskins, A review of indirect searches for particle dark matter, *Contemp. Phys.* **57**, 496 (2016), arXiv:1604.00014 [astro-ph.HE].
- [12] M. Cirelli, A. Strumia, and J. Zupan, Dark Matter (2024), arXiv:2406.01705 [hep-ph].
- [13] A. Boveia and C. Doglioni, Dark Matter Searches at Colliders, *Ann. Rev. Nucl. Part. Sci.* **68**, 429 (2018), arXiv:1810.12238 [hep-ex].
- [14] R. A. Flores and J. R. Primack, Observational and theoretical constraints on singular dark matter halos, *Astrophys. J. Lett.* **427**, L1 (1994), arXiv:astro-ph/9402004.
- [15] B. Moore, Evidence against dissipationless dark matter from observations of galaxy haloes, *Nature* **370**, 629 (1994).
- [16] J. S. Bullock and M. Boylan-Kolchin, Small-Scale Challenges to the Λ CDM Paradigm, *Ann. Rev. Astron. Astrophys.* **55**, 343 (2017), arXiv:1707.04256 [astro-ph.CO].
- [17] J. Zavala and C. S. Frenk, Dark matter haloes and subhaloes, *Galaxies* **7**, 81 (2019), arXiv:1907.11775 [astro-ph.CO].

- [18] W. Hu, R. Barkana, and A. Gruzinov, Cold and fuzzy dark matter, *Phys. Rev. Lett.* **85**, 1158 (2000), [arXiv:astro-ph/0003365](#).
- [19] A. Del Popolo and M. Le Delliou, Small scale problems of the Λ CDM model: a short review, *Galaxies* **5**, 17 (2017), [arXiv:1606.07790 \[astro-ph.CO\]](#).
- [20] D. J. E. Marsh and A.-R. Pop, Axion dark matter, solitons and the cusp–core problem, *Mon. Not. Roy. Astron. Soc.* **451**, 2479 (2015), [arXiv:1502.03456 \[astro-ph.CO\]](#).
- [21] R. G. García, P. Brax, and P. Valageas, Solitons and halos for self-interacting scalar dark matter, *Phys. Rev. D* **109**, 043516 (2024), [arXiv:2304.10221 \[astro-ph.CO\]](#).
- [22] P. Brax, J. A. R. Cembranos, and P. Valageas, Impact of kinetic and potential self-interactions on scalar dark matter, *Phys. Rev. D* **100**, 023526 (2019), [arXiv:1906.00730 \[astro-ph.CO\]](#).
- [23] P. Brax, J. A. R. Cembranos, and P. Valageas, Fate of scalar dark matter solitons around supermassive galactic black holes, *Phys. Rev. D* **101**, 023521 (2020), [arXiv:1909.02614 \[astro-ph.CO\]](#).
- [24] L. Hui, J. P. Ostriker, S. Tremaine, and E. Witten, Ultralight scalars as cosmological dark matter, *Phys. Rev. D* **95**, 043541 (2017), [arXiv:1610.08297 \[astro-ph.CO\]](#).
- [25] N. Bar, K. Blum, T. Lacroix, and P. Pani, Looking for ultralight dark matter near supermassive black holes, *JCAP* **07**, 045, [arXiv:1905.11745 \[astro-ph.CO\]](#).
- [26] E. Gross, Classical theory of boson wave fields, *Annals of Physics* **4**, 57 (1958).
- [27] E. P. Gross, Structure of a quantized vortex in boson systems, *Il Nuovo Cimento* **20**, 454 (1961).
- [28] L. P. PITAIEVSKII, Vortex lines in an imperfect bose gas, *Journal of Experimental and Theoretical Physics*, **13**, 451-454. **13**, 451-454. (1961).
- [29] C. Barenghi and N. G. Parker, *A Primer on Quantum Fluids* (2016).
- [30] N. Glennon, N. Musoke, E. O. Nadler, C. Prescod-Weinstein, and R. H. Wechsler, Dynamical friction in self-interacting ultralight dark matter, *Phys. Rev. D* **109**, 063501 (2024), [arXiv:2312.07684 \[astro-ph.CO\]](#).
- [31] G. Alonso-Álvarez, J. M. Cline, and C. Dewar, Self-Interacting Dark Matter Solves the Final Parsec Problem of Supermassive Black Hole Mergers, *Phys. Rev. Lett.* **133**, 021401 (2024), [arXiv:2401.14450 \[astro-ph.CO\]](#).
- [32] L. Teodori, A. Caputo, and K. Blum, Ultra-Light Dark Matter Simulations and Stellar Dynamics: Tension in Dwarf Galaxies for $m < 5 \times 10^{-21}$ eV, (2025), [arXiv:2501.07631 \[astro-ph.GA\]](#).
- [33] J. Antoniadis *et al.* (EPTA, InPTA:), The second data release from the European Pulsar Timing Array - III. Search for gravitational wave signals, *Astron. Astrophys.* **678**, A50 (2023), [arXiv:2306.16214 \[astro-ph.HE\]](#).
- [34] J. Antoniadis *et al.* (EPTA, InPTA), The second data release from the European Pulsar Timing Array - IV. Implications for massive black holes, dark matter, and the early Universe, *Astron. Astrophys.* **685**, A94 (2024), [arXiv:2306.16227 \[astro-ph.CO\]](#).
- [35] D. J. Reardon *et al.*, Search for an Isotropic Gravitational-wave Background with the Parkes Pulsar Timing Array, *Astrophys. J. Lett.* **951**, L6 (2023), [arXiv:2306.16215 \[astro-ph.HE\]](#).
- [36] A. Zic *et al.*, The Parkes Pulsar Timing Array third data release, *Publ. Astron. Soc. Austral.* **40**, e049 (2023), [arXiv:2306.16230 \[astro-ph.HE\]](#).
- [37] D. J. Reardon *et al.*, The Gravitational-wave Background Null Hypothesis: Characterizing Noise in Millisecond Pulsar Arrival Times with the Parkes Pulsar Timing Array, *Astrophys. J. Lett.* **951**, L7 (2023), [arXiv:2306.16229 \[astro-ph.HE\]](#).
- [38] G. Agazie *et al.* (NANOGrav), The NANOGrav 15 yr Data Set: Constraints on Supermassive Black Hole Binaries from the Gravitational-wave Background, *Astrophys. J. Lett.* **952**, L37 (2023), [arXiv:2306.16220 \[astro-ph.HE\]](#).
- [39] A. Afzal *et al.* (NANOGrav), The NANOGrav 15 yr Data Set: Search for Signals from New Physics, *Astrophys. J. Lett.* **951**, L11 (2023), [arXiv:2306.16219 \[astro-ph.HE\]](#).
- [40] H. Xu *et al.*, Searching for the Nano-Hertz Stochastic Gravitational Wave Background with the Chinese Pulsar Timing Array Data Release I, *Res. Astron. Astrophys.* **23**, 075024 (2023), [arXiv:2306.16216 \[astro-ph.HE\]](#).
- [41] G. Agazie *et al.* (International Pulsar Timing Array), Comparing Recent Pulsar Timing Array Results on the Nanohertz Stochastic Gravitational-wave Background, *Astrophys. J.* **966**, 105 (2024), [arXiv:2309.00693 \[astro-ph.HE\]](#).
- [42] M. C. Begelman, R. D. Blandford, and M. J. Rees, Massive black hole binaries in active galactic nuclei, *Nature* **287**, 307 (1980).
- [43] N. J. McConnell and C.-P. Ma, Revisiting the Scaling Relations of Black Hole Masses and Host Galaxy Properties, *Astrophys. J.* **764**, 184 (2013), [arXiv:1211.2816 \[astro-ph.CO\]](#).
- [44] E. S. Phinney, A practical theorem on gravitational wave backgrounds, [arXiv: astro-ph/0108028](#) (2001).
- [45] L. Hu, R.-G. Cai, and S.-J. Wang, Distinctive GWBs from eccentric inspiraling SMBH binaries with a DM spike, *JCAP* **02**, 067, [arXiv:2312.14041 \[gr-qc\]](#).
- [46] Y. Chen *et al.* (NANOGrav), Galaxy Tomography with the Gravitational Wave Background from Supermassive Black Hole Binaries, (2024), [arXiv:2411.05906 \[astro-ph.HE\]](#).
- [47] S. Chandrasekhar, Dynamical Friction. I. General Considerations: the Coefficient of Dynamical Friction, *Astrophys. J.* **97**, 255 (1943).
- [48] L. M. Widrow and N. Kaiser, Using the Schroedinger Equation to Simulate Collisionless Matter, *ApJ*, **416**, L71 (1993).
- [49] P. Coles and K. Spencer, A wave-mechanical approach to cosmic structure formation, *Mon. Not. Roy. Astron. Soc.* **342**, 176 (2003), [arXiv:astro-ph/0212433](#).
- [50] E. Y. Davies and P. Mocz, Fuzzy Dark Matter Soliton Cores around Supermassive Black Holes, *Mon. Not. Roy. Astron. Soc.* **492**, 5721 (2020), [arXiv:1908.04790 \[astro-ph.GA\]](#).
- [51] N. Bar, D. Blas, K. Blum, and S. Sibiryakov, Galactic rotation curves versus ultralight dark matter: Implications of the soliton-host halo relation, *Phys. Rev. D* **98**, 083027 (2018), [arXiv:1805.00122 \[astro-ph.CO\]](#).
- [52] S. Tremaine and J. E. Gunn, Dynamical Role of Light Neutral Leptons in Cosmology, *Phys. Rev. Lett.* **42**, 407 (1979).
- [53] L. Hui, Wave Dark Matter, *Ann. Rev. Astron. Astrophys.* **59**, 247 (2021), [arXiv:2101.11735 \[astro-ph.CO\]](#).
- [54] J. Kormendy and D. Richstone, Inward bound: The Search for supermassive black holes in galactic nuclei, *Ann. Rev. Astron. Astrophys.* **33**, 581 (1995).
- [55] J. Kormendy and L. C. Ho, Coevolution (Or Not) of Supermassive Black Holes and Host Galaxies, *Ann. Rev. As-*

- tron. *Astrophys. J.* **51**, 511 (2013), [arXiv:1304.7762 \[astro-ph.CO\]](#).
- [56] A. E. Reines, Hunting for massive black holes in dwarf galaxies, *Nature Astron.* **6**, 26 (2022), [arXiv:2201.10569 \[astro-ph.GA\]](#).
- [57] R. Ruffini and J. A. Wheeler, Introducing the black hole, *Phys. Today* **24**, 30 (1971).
- [58] W. Israel, Event horizons in static vacuum space-times, *Phys. Rev.* **164**, 1776 (1967).
- [59] W. Israel, Event horizons in static electrovac space-times, *Commun. Math. Phys.* **8**, 245 (1968).
- [60] B. Carter, Axisymmetric Black Hole Has Only Two Degrees of Freedom, *Phys. Rev. Lett.* **26**, 331 (1971).
- [61] J. D. Bekenstein, Transcendence of the law of baryon-number conservation in black hole physics, *Phys. Rev. Lett.* **28**, 452 (1972).
- [62] V. Cardoso, T. Ikeda, R. Vicente, and M. Zilhão, Parasitic black holes: The swallowing of a fuzzy dark matter soliton, *Phys. Rev. D* **106**, L121302 (2022), [arXiv:2207.09469 \[gr-qc\]](#).
- [63] E. Figueiredo, A. Maselli, and V. Cardoso, Black holes surrounded by generic dark matter profiles: Appearance and gravitational-wave emission, *Phys. Rev. D* **107**, 104033 (2023), [arXiv:2303.08183 \[gr-qc\]](#).
- [64] Z. Zhong, V. Cardoso, T. Ikeda, and M. Zilhão, Piercing of a solitonic boson star by a black hole, *Phys. Rev. D* **108**, 084051 (2023), [arXiv:2307.02548 \[gr-qc\]](#).
- [65] S. Chakrabarti, B. Dave, K. Dutta, and G. Goswami, Constraints on the mass and self-coupling of ultra-light scalar field dark matter using observational limits on galactic central mass, *JCAP* **09**, 074, [arXiv:2202.11081 \[astro-ph.CO\]](#).
- [66] V. Lora, J. Magana, A. Bernal, F. J. Sanchez-Salcedo, and E. K. Grebel, On the mass of ultra-light bosonic dark matter from galactic dynamics, *JCAP* **02**, 011, [arXiv:1110.2684 \[astro-ph.GA\]](#).
- [67] J. Barranco, A. Bernal, J. C. Degollado, A. Diez-Tejedor, M. Megevand, M. Alcubierre, D. Nunez, and O. Sarbach, Are black holes a serious threat to scalar field dark matter models?, *Phys. Rev. D* **84**, 083008 (2011), [arXiv:1108.0931 \[gr-qc\]](#).
- [68] J. Barranco, A. Bernal, J. C. Degollado, A. Diez-Tejedor, M. Megevand, M. Alcubierre, D. Nunez, and O. Sarbach, Schwarzschild black holes can wear scalar wigs, *Phys. Rev. Lett.* **109**, 081102 (2012), [arXiv:1207.2153 \[gr-qc\]](#).
- [69] H.-Y. Schive, M.-H. Liao, T.-P. Woo, S.-K. Wong, T. Chiueh, T. Broadhurst, and W. Y. P. Hwang, Understanding the Core-Halo Relation of Quantum Wave Dark Matter from 3D Simulations, *Phys. Rev. Lett.* **113**, 261302 (2014), [arXiv:1407.7762 \[astro-ph.GA\]](#).
- [70] K. Bandara, D. Crampton, and L. Simard, A Relationship between Supermassive Black Hole Mass and the Total Gravitational Mass of the Host Galaxy, *Astrophys. J.* **704**, 1135 (2009), [arXiv:0909.0269 \[astro-ph.GA\]](#).
- [71] A. Ghoshal and A. Strumia, Probing the Dark Matter density with gravitational waves from super-massive binary black holes, *JCAP* **02**, 054, [arXiv:2306.17158 \[astro-ph.CO\]](#).
- [72] M. Aghaie, G. Armando, A. Dondarini, and P. Pani, Bounds on ultralight dark matter from NANOGrav, *Phys. Rev. D* **109**, 103030 (2024), [arXiv:2308.04590 \[astro-ph.CO\]](#).
- [73] M. Maggiore, *Gravitational Waves. Vol. 1: Theory and Experiments* (Oxford University Press, 2007).
- [74] X.-J. Yue, W.-B. Han, and X. Chen, Dark matter: an efficient catalyst for intermediate-mass-ratio-inspiral events, *Astrophys. J.* **874**, 34 (2019), [arXiv:1802.03739 \[gr-qc\]](#).
- [75] J. A. Dror, B. V. Lehmann, H. H. Patel, and S. Profumo, Discovering new forces with gravitational waves from supermassive black holes, *Phys. Rev. D* **104**, 083021 (2021), [arXiv:2105.04559 \[astro-ph.CO\]](#).
- [76] W. DeRocco and J. A. Dror, Searching for stochastic gravitational waves below a nanohertz, *Phys. Rev. D* **108**, 103011 (2023), [arXiv:2304.13042 \[astro-ph.HE\]](#).
- [77] P.-H. Chavanis, Mass-radius relation of Newtonian self-gravitating Bose-Einstein condensates with short-range interactions: I. Analytical results, *Phys. Rev. D* **84**, 043531 (2011), [arXiv:1103.2050 \[astro-ph.CO\]](#).
- [78] D. G. Levkov, A. G. Panin, and I. I. Tkachev, Relativistic axions from collapsing Bose stars, *Phys. Rev. Lett.* **118**, 011301 (2017), [arXiv:1609.03611 \[astro-ph.CO\]](#).
- [79] A. R. Kaiser and S. T. McWilliams, Sensitivity of present and future detectors across the black-hole binary gravitational wave spectrum, *Class. Quant. Grav.* **38**, 055009 (2021), [arXiv:2010.02135 \[gr-qc\]](#).
- [80] J. Ellis, M. Fairbairn, G. Hütsi, M. Raidal, J. Urrutia, V. Vaskonen, and H. Veermäe, Prospects for future binary black hole gravitational wave studies in light of PTA measurements, *Astron. Astrophys.* **676**, A38 (2023), [arXiv:2301.13854 \[astro-ph.CO\]](#).
- [81] M. Colpi *et al.* (LISA), LISA Definition Study Report, (2024), [arXiv:2402.07571 \[astro-ph.CO\]](#).
- [82] A. Sesana, Insights into the astrophysics of supermassive black hole binaries from pulsar timing observations, *Class. Quant. Grav.* **30**, 224014 (2013), [arXiv:1307.2600 \[astro-ph.CO\]](#).
- [83] A. Sesana, F. Shankar, M. Bernardi, and R. K. Sheth, Selection bias in dynamically measured supermassive black hole samples: consequences for pulsar timing arrays, *Mon. Not. Roy. Astron. Soc.* **463**, L6 (2016), [arXiv:1603.09348 \[astro-ph.GA\]](#).
- [84] S. Chen, A. Sesana, and W. Del Pozzo, Efficient computation of the gravitational wave spectrum emitted by eccentric massive black hole binaries in stellar environments, *Mon. Not. Roy. Astron. Soc.* **470**, 1738 (2017), [arXiv:1612.00455 \[astro-ph.CO\]](#).
- [85] S. Chen, A. Sesana, and C. J. Conzelmann, Constraining astrophysical observables of Galaxy and Supermassive Black Hole Binary Mergers using Pulsar Timing Arrays, *Mon. Not. Roy. Astron. Soc.* **488**, 401 (2019), [arXiv:1810.04184 \[astro-ph.GA\]](#).
- [86] M. Bernardi, A. Meert, V. Vikram, M. Huertas-Company, S. Mei, F. Shankar, and R. K. Sheth, Systematic effects on the size-luminosity relation: dependence on model fitting and morphology (2012).